Chapter I.4
Introduction to SODAR and RASS-Wind Profiler Radar Systems

Laura Bianco

1 Introduction

We will start this overview by introducing Doppler radar wind profilers and then expand the discussion to RASS and SODAR systems later in the chapter.

Doppler radars have been used largely in the field of atmospheric research; however, during the first half of the last century, their use was focused mainly on the survey of the echoes obtained from visible structures. To find applications of radars in the study of the clear-air atmosphere, we have to go back to the late 1960s, when attention was focused on the determination of the causes of radar returns from apparently clear-air atmosphere (often referred to as "angels"). The first idea was that those echoes were of biological origin (insects or birds), but subsequent research (Hardy et al., 1966; Kropfli et al., 1968; Lane, 1969) established that, though point sources also provide natural targets, scattering from turbulent irregularities (refractive index inhomogeneities) is the primary cause of clear-air echoes observed at microwave frequencies. Radars designed specifically to sound the clear air were then built (Richter, 1969) and demonstrated unequivocally that clear-air radars could routinely observe profiles of refractive index inhomogeneities. Refractive index fluctuations are carried out by the wind, so they are used as tracers. During subsequent years many results were added to the first applications, making the ability of those radars well established and their use very diffuse. Radars transmit radio frequency energy, which is intercepted and reradiated by land, sea, and atmospheric targets (Fig. I.4.1). Changes in the received signal from that transmitted give clues to important target parameters, such as scattering cross sections as well as their position, as a function of time, in three-dimensional space. Thus, their velocity can be determined.

Doppler radars can operate over a wide range of frequencies, in the VHF (30–300 MHz) and UHF (300–30,000 MHz). According to the Bragg condition the scale of the backscattering target toward the point of origin occurs primary from

L. Bianco (✉)
Cooperative Institute for Research in Environmental Sciences (CIRES),
University of Colorado, Boulder, CO, USA; NOAA/Earth System Research Laboratory
(ESRL)/Physical Sciences Division (PSD), Boulder, CO, USA
e-mail: laura.bianco@noaa.gov

D. Cimini et al. (eds.), *Integrated Ground-Based Observing Systems*,
DOI 10.1007/978-3-642-12968-1_4,

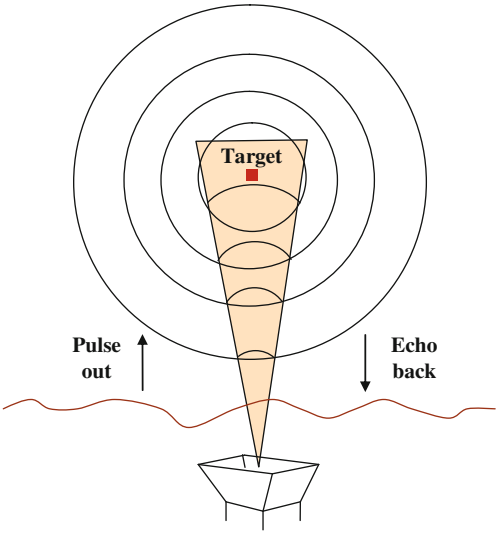

Fig. I.4.1 Scattering from target (adapted from the wind profiler manual)

irregularities of size and on the order of one-half the wavelength of the incident wave. Being capable of retaining information on the phase of the signal returns, Doppler radars are used to measure the frequency spectrum of the incoming signal. Using the principles of the Doppler effect, they are capable of measuring the mean radial component of motion of the scattering elements. The mean Doppler shift (first moment) is a measure of the mean radial component of motion of the scattering element. Furthermore, the magnitude of the echo spectrum (zeroth moment) and the width of the Doppler spectrum (second moment) contain additional information on wind shear, turbulence parameters (White, 1997), and boundary layer structure (Bianco et al., 2008).

The class of radars using fixed-beam-pointing directions is then able to determine the characteristics of the wind vector (speed and direction), and, for this reason, they became to be known as *wind profilers*. Among them UHF radar wind profilers are specifically designed for boundary layer and lower-tropospheric studies (Ecklund et al., 1988).

2 Basic Theory of Doppler Radars

The echoing mechanisms that give rise to backscattering from the clear-air atmosphere have been rather extensively investigated. The main cause of radar returns from the clear air now has been well established to be the inhomogeneities in refractive index that result from turbulence. The radio refractive index n, at commonly used radar wavelengths, is non-dispersive and depends on the atmospheric temperature, humidity, and pressure.

It can be expressed in terms of the *refractivity* $N = (n-1) \times 10^6$ as

$$N = (n-1) \times 10^6 = 77.6\frac{p}{T} + 3.73 \times 10^5 \frac{e}{T^2}, \tag{1}$$

where p is the atmospheric pressure (mb), e is the vapor pressure (mb), and T is the absolute temperature (K).

2.1 Radar Principles

Let a pulsed electromagnetic wave be transmitted at time T_1, the pulse duration of this radar being τ. For simplification the pulse shape is supposed to be rectangular, but in real applications it may be a smoothed trapezoid or triangle or Gaussian shaped. In a non-dispersive propagation medium the pulse travels with the speed of the light c and reaches the range r_a after time $t_1 = r_a/c$. A target at r_a can scatter or reflect the radar signal in some directions. A small fraction returns to the location of the transmitter, where the radar echo will be received after time $t_2 = 2t_1 = 2r_a/c$. This yields the basic relation $r = c \cdot t/2$, which allows the determination of the range r of any radar target by measuring the round-trip time t. This relation holds for monostatic radars (transmitter and receiver are at the same location). For bistatic radars (receiver separated from transmitter by a distance comparable to or larger than the ranges to the target), a modified expression has to be applied.

Since the transmitted pulse has a finite duration τ, its trailing edge will reach the range r_a at a time $t_1 + \tau$ and reach the receiver at $t_2 + \tau$. The pulse of duration τ, thus, at one time illuminates a volume at r_a extended along a range $\Delta r = c \cdot \tau/2$. This is the *range gate* from which the radar echoes are received. Therefore, the transmitter pulse length τ determines the *range resolution* Δr. In contrast, the horizontal size of the scattering volume is obviously defined by the antenna beam width.

In radar applications short pulses are normally transmitted periodically, so that the nth pulse follows the $(n-1)$th pulse after a specific time. This time $(T_n - T_{n-1})$ is called the *interpulse period*, T_{IPP}. Its inverse is called the *pulse repetition frequency*, $f_{\mathrm{PRF}} = 1/T_{\mathrm{IPP}}$. The off–on ratio of the transmitter $T_{\mathrm{IPP}}/\tau - 1$ determines approximately the range from which radar echoes can be unambiguously received (in unit of range resolution). It is more customary, however, to use the ratio $d = \tau/T_{\mathrm{IPP}}$, which is called *duty cycle*.

Because in normal radar operations the pulse repetition frequency is kept constant (the transmitted pulse train is periodic), range aliasing may occur. At time t_a an echo is received from the range r_a, and an echo is received from range r_b. Of course higher-order range aliasing can occur from ranges $r_n = c \cdot (t + (n-1)\,T_{\mathrm{IPP}})/2$. Because these echoes return from separate scatter volumes, the echo signals are uncorrelated, but still their power accumulates in the same receiver range gate. If special arrangements are not being made (i.e., pulse-coding), the maximum unambiguous range is $r_{\max} = c \cdot T_{\mathrm{IPP}}/2$. The minimum range $r_{\min}$ is obviously given by

the pulse duration τ, $r_{\min} = c \cdot \tau / 2$, plus some instrumentally determined transition time between transmission and reception.

A point target within the scattering volume defined by the antenna beam width and pulse duration τ returns a signal whose instantaneous voltage is

$$E(t) = A(t) \cos[\omega_c t + \varphi(t)], \tag{2}$$

where A is the amplitude, $\omega_c = 2\pi f_c$ is the constant carrier frequency, and φ is the phase relative to the carrier phase. If the target is fixed, the phase is constant and a function of the distance r from the radar. A moving target having a radial velocity V_R returns a signal whose phase varies with time and is given by

$$\varphi(t) = \frac{4\pi}{\lambda}(r_0 + V_R t), \tag{3}$$

where λ is the incident radiation wavelength and r_0 is the initial distance.

When the scattering volume contains N point targets, the return signal is the superimposition of individual returns. The instantaneous return voltage is then

$$E(t) = \sum_{n=1}^{N} A_n(t) \cos[\omega_c t + \varphi_n(t)], \tag{4}$$

where A_n is the amplitude and φ_n is the phase of the return signal from the nth scatterer. The above expression assumes that secondary scattering effects are negligible compared to the first-order scattering. With the possible exception of heavy rain, snow, or hail, the above expression is valid for atmospheric scattering.

The time rate of phase exchange, time derivative of Eq. (3), is an angular frequency $\omega_D = 4\pi V_R / \lambda$. It is therefore equivalent to a Doppler frequency shift

$$f_D = \frac{2V_R}{\lambda}. \tag{5}$$

Approaching targets have increasing phase with time, which corresponds to a positive Doppler frequency shift.

In a pulsed Doppler radar system, the time functions for point [Eq. (2)], or for distributed targets [Eq. (4)], are available only at discrete time intervals corresponding to the radar pulse repetition period. Therefore, if the radial velocity of the scatterers is such that the phase changes by more than π (Doppler frequency shift greater than one-half the pulse repetition rate), an ambiguity in velocity exists. This is equivalent to aliasing at the folding or Nyquist frequency given by

$$f_N = \frac{1}{2T_{IPP}}, \tag{6}$$

where T_{IPP} is the pulse repetition period or interpulse period. If positive and negative frequencies can be resolved, the unambiguous frequency range is doubled.

The unambiguous Doppler frequency range is then

$$-\frac{1}{2T_{\mathrm{IPP}}} \leq f_{\mathrm{D}} \leq \frac{1}{2T_{\mathrm{IPP}}}. \tag{7}$$

From the previous equation, the maximum unambiguous velocity is then

$$V_{\max} = \pm\frac{\lambda}{4T_{\mathrm{IPP}}}. \tag{8}$$

2.2 The Radar Equation

A target having a cross-sectional area A_{c} located at a distance r from the radar will intercept an amount of power,

$$P_{\mathrm{i}} = \frac{P_{\mathrm{t}} G A_{\mathrm{c}}}{4\pi r^2}, \tag{9}$$

where P_{t} is the transmitted power and G is the transmitting antenna gain factor (Barrick, 1972). If the target reradiates isotropically, the power intercepted by the receiving antenna is (Battan, 1959)

$$P_{\mathrm{r}} = \frac{P_{\mathrm{t}} G A_{\mathrm{c}}}{4\pi r^2}\frac{A_{\mathrm{e}}}{4\pi r^2} \tag{10}$$

for a receiving antenna having an effective area A_{e}. The relationship between effective area and its gain is (Kraus 1950)

$$A_{\mathrm{e}} = \frac{G\lambda^2}{4\pi}. \tag{11}$$

Since most targets do not scatter isotropically, it is convenient to introduce the backscattering cross section σ, defined as (Battan 1959) "the area intercepting the amount of power, which, if scattered isotropically, would return an amount of power equal to that actually received"; that is

$$\sigma = \frac{(\text{Power reflected toward the receiving aperture per unit solid angle})}{(\text{Incident power density per } 4\pi \text{ steradians})}.$$

Substituting the backscattered cross section for the geometric cross section and replacing the effective area with Eq. (11), the return power [Eq. (10)] becomes

$$P_{\mathrm{r}} = K_{\mathrm{r}}\frac{\sigma}{r^4}, \tag{12}$$

where the constant $K_r = P_t G^2 \lambda^2 / 64\pi^3$ depends only on the particular radar system used and not on the scatterers.

For N targets, where σ_n is the cross section for the nth scatterer, on average, the return power is

$$\overline{P_r} = \frac{K_r}{r^4} \sum_{n=1}^{N} \sigma_n, \tag{13}$$

where r is the range to the center of the scattering volume. A slightly more useful meteorological form is obtained by using the average radar cross section per unit volume and multiplying by the volume, V, effectively illuminated. This leads to

$$\overline{P_r} = \frac{K_r V \eta}{r^4}. \tag{14}$$

The quantity

$$\eta = \frac{1}{V} \sum_{n=1}^{N} \sigma_n \tag{15}$$

is the so-called *radar reflectivity*.

Approximating the antenna pattern by a Gaussian beam (Lhermitte, 1963; Nathanson and Reilly, 1968), the gain is

$$G(\vartheta, \alpha) = G_0 \exp\left[-\left(\frac{\vartheta^2}{2\sigma_\vartheta^2} + \frac{\alpha^2}{2\sigma_\alpha^2} \right) \right], \tag{16}$$

where $\sigma_\vartheta, \sigma_\alpha$ are the standard deviations of the two-way pattern (assumed to be at most a few degrees), ϑ and α are, respectively, the off-axis horizontal and vertical beam angles (assumed to be at most a few degrees), and G_0 is the on-axis gain factor. Accounting for gain variations across the beam, the exact form of the radar equation [Eq. (13)] becomes

$$\overline{P_r} = \frac{P_t \lambda^2}{64\pi^3} \sum_{\text{vol}} \frac{G^2(\vartheta, \alpha)\, \sigma_n}{r_n^4}. \tag{17}$$

Introducing the radar reflectivity $\eta = \eta(r, \vartheta, \alpha)$, the summation can be expressed as a volume integral over the pulse of the contribution region so that

$$\overline{P_r} = \frac{P_t \lambda^2}{64\pi^3} \int_{\text{vol}} \frac{G^2(\vartheta, \alpha)\, \eta(r, \vartheta, \alpha)}{r^4} dV. \tag{18}$$

Using the Gaussian beam approximation over a volume having uniform reflectivity, integration leads to (Probert-Jones, 1960)

$$\overline{P_{\mathrm{r}}} = \frac{c}{1024\pi^2 \ln 2} \left(P_{\mathrm{t}} \tau \lambda^2 G_0^2 \vartheta \alpha\right) \left(\frac{\eta}{r^2}\right), \tag{19}$$

where τ is the pulse width and c is the propagation speed ($\cong 3 \times 10^8$ ms^{-1}).

The previous equation has been grouped according to the constant $\left(c/\left(1024\pi^2 \ln 2\right)\right)$, the measurable radar parameters $\left(P_{\mathrm{t}} \tau \lambda^2 G_0^2 \vartheta \alpha\right)$, and target parameters $\left(\eta/r^2\right)$.

2.3 Method of Wind Measurement

Here we describe the standard technique.

Wind-profiling radars have five possible beam directions (Fig. I.4.2), any one of which having a beam width equal to 3–10° and tilted 14–24° with respect to the vertically pointing beam. Four beams are orthogonal. The beam-pointing sequence is repeated every 1–5 min while local horizontal uniformity of the wind field is assumed.

Wind-profiling radars use fixed-pointing antennas with three or five pointing directions. At least three antenna beam-pointing directions are needed to measure the vector wind. Let us consider a Doppler radar using three antenna beam-pointing directions (Fig. I.4.3).

For simplicity two pointing directions are chosen to observe orthogonal horizontal wind components u and v, and one is chosen to observe the vertical component w. Thus, one antenna beam is pointed vertically and the other two are oblique. Horizontal winds are measured with an antenna elevation-pointing angle

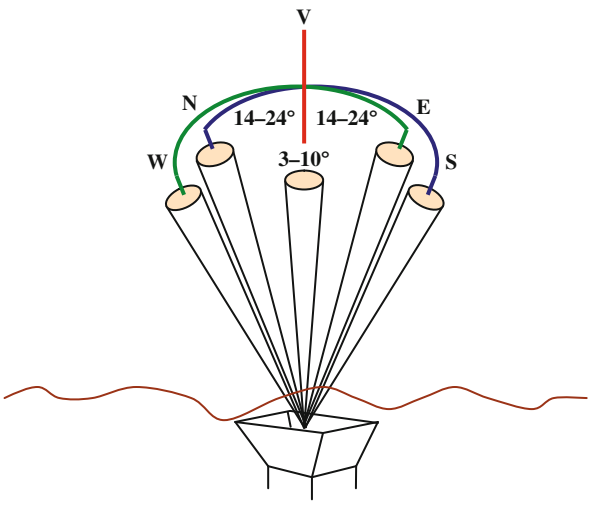

Fig. I.4.2 Possible wind directions for a wind-profiling radar (adapted from the wind profiler manual)

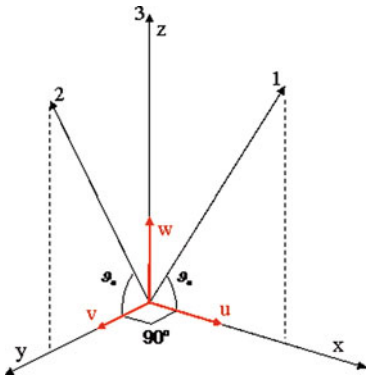

Fig. I.4.3 Wind measurement method

ϑ_e that allows observation at all altitudes of interest. If we consider for simplicity that the azimuth angles for the oblique beams are equal to 0° and 90°, respectively, we obtain that the radar Doppler velocity V_i measured along axes 1, 2, and 3 by the radar is related to the wind as follows:

$$\begin{cases} V_1 = u\cos\vartheta_e + w\sin\vartheta_e \\ V_2 = v\cos\vartheta_e + w\sin\vartheta_e \\ V_3 = w \end{cases} . \tag{20}$$

At each altitude h the three measurements are made at volumes separated in space. Again, horizontal uniformity is assumed when the measurements are combined.

2.4 Data Processing and Averaging

Wind-profiling radars use the data processing scheme illustrated in Fig. I.4.4 (Strauch et al., 1984).

Steps (1) and (2). The input signal is the backscattered signal for each radar resolution volume. Signal-plus-noise values are collected by the receiver and sampled.

Step (3). The next step in signal processing is coherent integration, also referred to as time-domain average. The signal-to-noise ratio (SNR) can be improved for radar wind profiling by summing a number J of consecutively received pulses. Since the noise bandwidth is determined by the radar pulse width, noise samples taken at the pulse repetition period will be uncorrelated. Therefore, the noise power increases linearly with the number of samples added. The signal, however, remains well correlated for approximately $0.2\lambda/\sigma$ s (Nathanson, 1969), where λ is the radar wavelength. Typically $\sigma \cong 1$ ms^{-1}, so the correlation time is milliseconds with microwave radars. If, in addition to being correlated, the phase of the signal samples changes very little between samples, then signal samples can be added so that

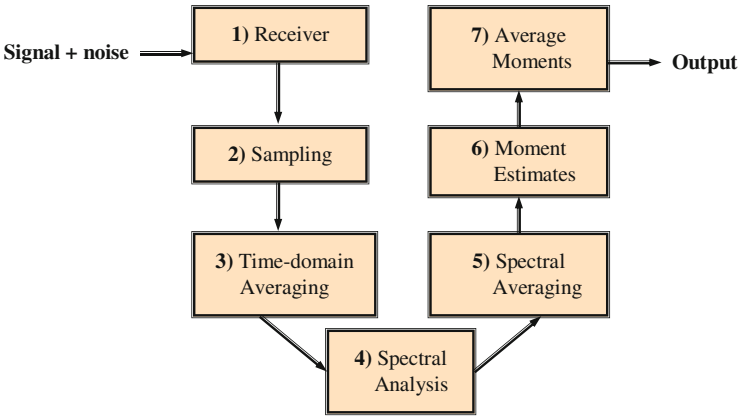

Fig. I.4.4 "Data processing" steps for a Doppler wind-profiling radar

signal power increases with the square of the number of samples added. This occurs for radars whose unambiguous velocity, Eq. (8), is much greater than the radial velocity of the scatterers. The SNR improves by the number J of samples averaged, and the unambiguous velocity [Eq. (8)] decreases to

$$V_{\max} = \pm \frac{\lambda}{4JT_{\mathrm{IPP}}}. \tag{21}$$

Step (4). Next is the computation of the power spectrum over a set of N_{FFT} coherent integrations. The program applies a standard fast Fourier transform (FFT) to the complex sample points from the decoded input array for each range gate. The number of FFT points can be any power of 2 from 8 to 4,096. The direct current (DC) component is zeroed out and the transform is then interpolated across DC. In a more recent version of the radar control program, the long-term mean value at DC is subtracted from the transform. Next, a frequency-domain Hanning window is applied to reduce the effects of spectral leakage caused by using time series of finite length. The program forms the power spectrum by computing the magnitude squared of the FFT array. The process is repeated until the specific number L of spectra is accumulated for each range gate.

Step (5). Next is the averaging of L spectra, each obtained from $J \times N_{\mathrm{FFT}}$ radar pulses. We expect averaging to improve the spectral domain SNR; however, this improvement will occur only if the mean wind is the same for each *dwell time*. The dwell time is the time required to collect and process $J \times N_{\mathrm{FFT}} \times L$ pulses. Thus, it is defined in terms of the number of spectra averaged L, the number of FFT points, N_{FFT}, the interpulse period T_{IPP}, and the number of pulses averaged J as

$$t_{\mathrm{D}} = L \times (N_{\mathrm{FFT}} \times T_{\mathrm{IPP}} \times J + t_0)\,, \tag{22}$$

where t_0 represent a constant for processing time ($\cong 0.5$ s).

In the standard method, before calculating the moments of the spectral signal, the program attempts to identify the spectral components caused by ground clutter which is a form of radar contamination (Riddle and Angevine, 1992). Ground clutter occurs when fixed objects on and near the earth's surface obstruct the radar beam and produce non-meteorological echoes with large intensities centered over zero shifts Doppler.

If there is a symmetrical signal peak centered on the DC point, it is assumed to be ground clutter and that region is excluded from the search for an atmospheric signal. This ground clutter algorithm starts at the operator-specified height and works downward. In order to avoid confusion with low velocity and signals, the ground clutter algorithm is not applied at a range gate if the signal at the height above is near zero velocity. At this stage of the process other methods can be applied to remove further non-atmospheric contamination to the spectral signal.

Step (6). The next step is the estimation of the spectral moments from the average Doppler velocity spectrum corrected by ground clutter influences and additional contamination. Before the moments can be found, the signal spectrum must be isolated from the measured signal-plus-noise spectrum. To achieve this aim, first the mean noise level is found. The algorithm for this calculation is based on the statistical property of Gaussian white noise that the variance of the spectral points should be equal to their squared mean value divided by the number of spectral averages. The program finds the largest number of the lowest-valued spectral points that exhibit the above statistics (Hildebrand and Sekhon, 1974). The noise level of the spectrum is the average of these points.

The signal is then identified within the spectrum by finding the spectral point outside the clutter region that has the maximum power. The signal region is identified to include all contiguous points around this peak that are both above the noise level and outside the clutter bounds. Next, the noise level is subtracted from all points within the signal bounds. The zeroth (power), first (mean Doppler velocity), and second moments are then calculated for the resulting power distribution as schematically illustrated in Fig. I.4.5. The spectral width is twice the square root of the second moment.

This method appears to work well for a wide variety of conditions.

Step (7). The program saves the mean Doppler values for later use in computing an average wind vector at each range gate. The winds are derived from a consensus average of the radial velocities over the chosen averaging interval (typically 30–60 min). The consensus-averaging algorithm examines the velocity values at each range gate and finds the largest subset of values that are within a specified velocity interval of each other (Strauch et al. 1984). If that subset contains less than a preselected percentage of the total values, then the data are rejected for that height. Both the velocity interval (consensus window) and the required percentage (consensus threshold) can be selected by the operator. An average signal-to-noise ratio is associated with each consensus average by averaging the SNR for all the records that were accepted for the radial velocity consensus average. After the consensus-averaged radial velocities are computed for each radar beam position, an average

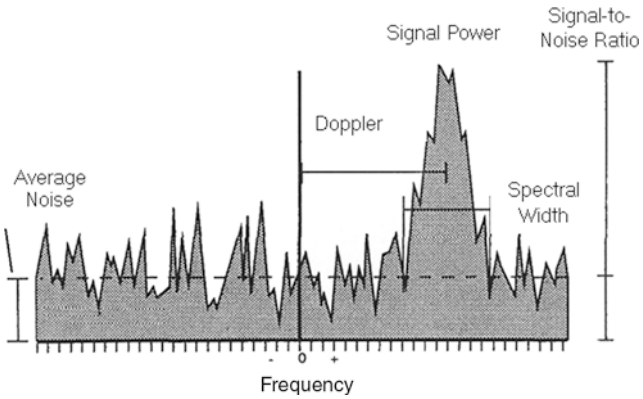

Fig. I.4.5 Example of Doppler spectrum. The x-axis is the radial velocity in ms-1. The y-axis is the signal power normalized to the maximum value of the spectrum. The 0th moment is the mean amplitude of the peak above the noise. The Doppler shift is the 1st moment. The spectral width is twice the square root of the 2nd moment (adapted from the wind profiler manual)

Table I.4.1 Typical specifications for commercially available radar wind profilers

Typical specifications	Lower-tropospheric radar	Mid-tropospheric radar	Tropospheric radar (1)	Tropospheric radar (2)
Operating frequency (MHz)	915 or 1290	449	46–68	449 or 482
Minimum height (m)	120	200–300	500–1,000	400
Maximum height (km)	up to 3	up to 8	up to 16	up to 16
Vertical range resolution (m)	60, 100, 200, 400	100–1,000	150–1,000	250–1,000
Wind-speed accuracy (m/s)	<1	<1	<1	<1
Wind-direction accuracy (°)	<10	<10	<10	<10
Wind-averaging time (min)	3–60	5–60	5–60	3–60
Antenna	Type electrically steerable micropatch-phased array panels	Type electrically steerable coaxial collinear array	Type electrically steerable array of 144 3-element Yagi-Uda antennas	Type electrically steerable coaxial colinear array

horizontal wind vector is calculated. The operator has the option of using the vertical beam consensus value to correct for a vertical wind component in the off-vertical beam radial velocities. From these corrected and combined radial velocity values, the wind components u, v, and w (or speed and direction) are then computed.

Typical specifications for commercially available lower-tropospheric, mid-tropospheric, and tropospheric radar wind profilers are presented in Table I.4.1 (http://www.vaisala.com/weather/products/windprofilers).

A Doppler radar wind profiler can be configured to sample in more than one mode. Those are referred to as "low mode" (smaller vertical range resolution) and "high mode" (larger vertical range resolution). The greater vertical resolution increases the maximum altitude to which the radar wind profiler can sample, but at the expense of coarser vertical resolution and an increase in the altitude at which the first winds are measured. When radar wind profilers are operated in multiple modes, the data are often combined into a single overlapping data set to obtain a better picture of the atmosphere.

3 RASS

The remote measurement of temperature in the lower atmosphere has been achieved with the development of a Radio Acoustic Sounding System (RASS) co-located with the radar wind profilers, through whom a longitudinal acoustic wave propagates upward in the air as a local compression and rarefaction of the ambient air. These density variations cause a corresponding variation in the local refractive index of the atmosphere, tracked by the Doppler radar through the reflection of a small amount of the electromagnetic energy as it propagates through the acoustic pulse. RASS is hence used to measure the speed of sound at various heights above the ground. Though only a small fraction of the electromagnetic energy is reflected, advantage is taken of two phenomena to increase the reflected signal (North and Peterson, 1973).

(1) The acoustic source and radar are located close together so that the spherical wavefronts from each are close to being in coincidence, and energy reflected from the entire acoustic wave is focused at the receiver.
(2) An acoustic pulse consisting of many cycles can be transmitted, resulting in scattering of the electromagnetic energy from successive wavefronts. Furthermore, when the acoustic wavelength, λ_a, is made one-half of the electromagnetic wavelength λ, the energy reflected from each acoustic wavefront adds coherently at the receiver, greatly increasing the return signal strength. The condition $\lambda_a = \lambda/2$ is basically the Bragg scattering condition.

From the measure of the speed of sound, the temperature in the boundary layer can be measured. Under the ideal gas assumption in fact, the speed of sound through dry still air of average atmospheric composition is given by

$$v_S = \sqrt{\frac{\gamma RT}{M}} = H\sqrt{T}, \tag{23}$$

where γ is the ratio of specific heats, R the gas constant, and M the apparent molecular weight, all for an ideal gas having the composition of the average dry atmosphere, and T is the temperature in Kelvin. H is a parameter that varies with humidity. For this reason RASS basically provides profiles of a virtual temperature that is a temperature uncompensated for humidity or pressure. The formal definition of virtual temperature is "the temperature that dry air would have if its pressure and specific volume were equal to those of a given sample of moist air." This parameter allows meteorologists to use the equation of state for dry air even though moisture is present. The equation for the virtual temperature as a function of temperature and mixing ratio is

$$T_{\mathrm{v}} = T\,(1 + 0.61r) \tag{24}$$

where T_{v} is the virtual temperature in Kelvin and r is the mixing ratio.

The data processing and analysis for RASS acquisitions are developed in a similar manner to that of the radar. For that which concerns the estimation of the moments, there is the added feature that two sets of moments are computed. Two separate signals are identified for each RASS spectrum: one for the acoustic return signal at a Doppler shift corresponding to the speed of sound and the other for the wind signal in the lower-velocity region of the spectrum. Since a RASS spectrum has two sets of moments associated with it, three consensus averages are computed. The first is the consensus average of the acoustic signal radial velocity, the second is the consensus average of the wind radial velocity, and the third is the consensus average of the difference between the acoustic and the wind velocities. The average corrected and uncorrected acoustic speeds are then converted to virtual temperature values. The standard RASS retrieval formula is (Angevine et al., 1998)

$$T_{\mathrm{v}} = \frac{c_{\mathrm{a}}^2}{401.92} - 273.16, \tag{25}$$

where T_{v} is the virtual temperature (°C) and c_{a} is the acoustic velocity corrected for vertical wind w.

The maximum height of the RASS signal is determined principally by the radar wavelength and the temperature and moisture structure of the atmosphere. For typical midlatitude conditions, a UHF 915-MHz profiler/RASS system will usually provide temperature measurements to 0.5–1.0 km. In a moist boundary layer the maximum height is generally above 1 km (Wilczak et al., 1996).

Figure I.4.6 shows the 1,290-MHz Doppler radar wind profiler, equipped with a RASS located in Assergi (L'Aquila), Italy.

Typical specifications for commercially available RASS associated with lower-tropospheric, mid-tropospheric, and tropospheric radar wind profilers (http://www.vaisala.com/weather/products/windprofilers) are presented in Table I.4.2.

Fig. I.4.6 Picture of the wind profiler – RASS system located on the top of one building of the National Laboratory of Gran Sasso (LNGS), at an altitude of 981 m ASL. It works at 1,290 MHz, relative to a wavelength of about 23 cm

Table I.4.2 Typical specifications for commercially available RASS associated with radar wind profilers

Typical specifications	RASS/lower-tropospheric radar	RASS/mid-tropospheric radar	RASS/ tropospheric radar (1)	RASS/ tropospheric radar (2)
Minimum height (m)	120	200–300	500–1,000	400
Maximum height (km)	Up to 1.5	Up to 2.5	Up to 5	Up to 5
Vertical range resolution (m)	60, 100, 200, 400	100–1,000	150–1,000	250–1,000
Temperature accuracy (°C)	1	1	1	1
Temperature averaging time (min)	3–60	3–60	5–60	3–60
Audio frequency	2–4 kHz, Bragg matched to transmitter frequency	∼1 kHz, Bragg matched to transmitter frequency	80–150 Hz, Bragg matched to transmitter frequency	∼1 kHz, Bragg matched to transmitter frequency

4 SODAR

SOund Detection And Ranging (SODAR) is a weather observing device that uses sound waves to detect the wind speed and direction at various elevations above the ground (Konrad et al., 1974; Spizzich, 1974; Spizzichino, 1974). The difference between SODARs and wind-profiling radars is that acoustic signals are used rather than electromagnetic signals to remotely sense winds aloft. In a typical implementation, the SODAR can sample along each of the three beams: one is aimed vertically to measure vertical velocity, and two are tilted off vertical and oriented orthogonal to one another to measure the horizontal components of the air's motion (Fig. I.4.7).

Pulses are transmitted consecutively along each of the three beam axes at slightly different frequencies to avoid overlapping of the signal. Again, using appropriate trigonometry, the three-dimensional meteorological velocity components (u, v, and w) and wind speed and wind direction are calculated from the radial velocities with corrections for vertical motions. A profile of the atmosphere as a function of height can be obtained by analyzing the return signal at a series of times following the transmission of each pulse. The return signal recorded at any particular delay time provides atmospheric data for a height that can be calculated based on the speed of sound. In this case the pulse frequency is chosen as a good compromise between the attenuation of the signal (which increases with the frequency) and the environmental noise. The attenuation of propagating acoustic energy increases as a function of increasing frequency, decreasing temperature, and decreasing humidity.

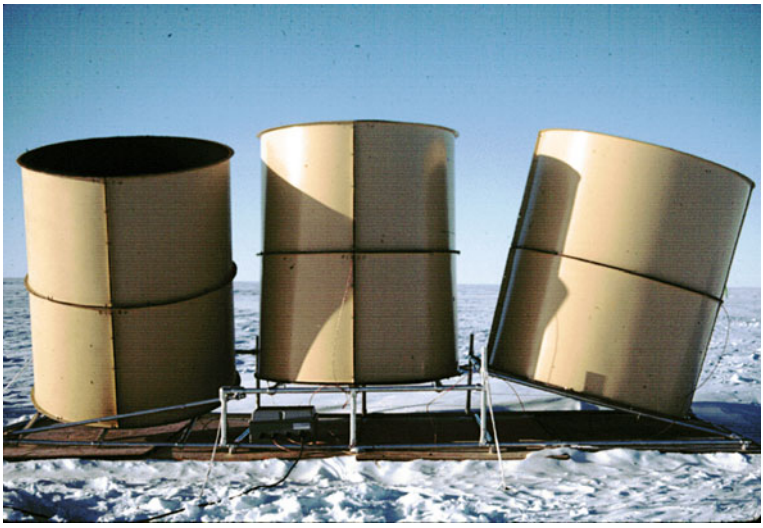

Fig. I.4.7 Picture of a SODAR system with three beam directions

For any transmitted pulse, the received Doppler frequency is computed and converted in wind velocity through the relation:

$$v = \frac{c_a}{2}\left(\frac{f_d}{f_0}\right), \tag{26}$$

where c_a is the sound velocity, f_d the Doppler shift, and f_0 the frequency of the pulse. For example, if $f_0 = 2,000\,\text{Hz}$ we will have a shift equal to 12 Hz in frequency for every ms^{-1} of wind velocity.

4.1 Data Processing and Averaging

Signal processing is another area where SODAR systems are rather similar to radar wind profilers. Again, SODAR systems use a fast Fourier transform (FFT) to derive the signal Doppler shift, but a variety of techniques may be used both before and after FFT processing to improve signal detection. One technique is to average the signal. Signal averaging may be used either in the time domain (before FFT) or in the frequency domain (after FFT) in an attempt to reduce noise level and improve the SNR, which is usually the primary criterion for data acceptance. Data storage and presentation capabilities can be different from system to system. Most systems will provide both text and plotted data showing the profiles of the horizontal and vertical winds and a facsimile display showing intensity data. The individual wind component data may also be provided, which can be very useful for quality control purposes. Data pertaining to signal quality are also usually displayed and recorded. The SNR is normally provided, but there is no common definition of this among SODAR manufacturers. Due to the large volume of data generated by a SODAR system, usually only the data averages are recorded and not the raw input signal.

As for radar wind profilers, one of the most important problems with SODAR systems is ground clutter. Its interference occurs when side-lobe energy radiating from a SODAR antenna on transmit is reflected back to the antenna by nearby fixed objects such as buildings, trees, mountains, or towers. This reflected side-lobe energy can overcome the atmospheric return signal. For this reason, SODAR systems must either be located in areas with no reflecting objects in the area, or they must be designed to substantially eliminate side-lobe energy.

Typical SODAR specifications are introduced in Table I.4.3.

Table I.4.3 Typical specifications for commercially available SODAR systems

	Performances
Height coverage	25–1,500 m
Vertical resolution	13–50 m
Accuracy	$\pm$ 0.2 ms^{-1}
Used frequencies	1,750–2,000–2,250 Hz
Acoustic power	50 W
Geometry	Monostatic

References

Angevine WM, Bakwin PS, Davis KJ (1998) Wind profiler and RASS measurements compared with measurements from a 450-m tall tower. J Atmos Ocean Technol 15:818–825

Barrick DE (1972) Remote sensing of sea state by radar. In: Derr VE (ed) Remote sensing of the troposphere. US Government Printing Office, Washington, DC

Battan LJ (1959) Radar meteorology. University of Chicago Press, Chicago, IL, 161 pp

Bianco L, Wilczak JM, White AB (2008) Convective boundary layer depth estimation from wind profilers: statistical comparison between an automated algorithm and expert estimations. J Atmos Ocean Technol 25:1397–1413

Ecklund WL, Carter DA, Balsley BB (1988) A UHF wind profiler for the boundary layer: brief description and initial results. J Atmos Ocean Technol 5:432–441

Hardy KR, Atlas D, Glover KM (1966) Multiwavelength backscatter from the clear atmosphere. J Geophys Res 71:1537–1552

Hildebrand PH, Sekhon, RS (1974) Objective determination of the noise level in Doppler spectra. J Appl Meteorol 13:808–818

Konrad TG, Arnold A, Dobson EB et al (1974) Unique boundary-layer experiment using radar, SODAR, and instrumented aircraft. EOS Trans-Am Geophys Union 55:271

Kraus JD (1950) Antennas. McGraw-Hill, New York, NY, 553 pp

Kropfli RA, Katz I, Konrad TG, Dobson EB (1968) Simultaneous radar reflectivity measurements and refractivity index spectra in the clear atmosphere. Radio Sci 3:991–994

Lane JA (1969) Radar echoes from clear air in relation to refractive-index variations in the troposphere. Proc. IRE Lond 116:1656–1660

Lhermitte RM (1963) Motion of scatterers and the variance of the mean intensity of weather radar signals. Sperry Rand Res. Rept. No. SRRC-RR-63-57. Sperry Rand Res. Center, Sudbury. 43 pp

Nathanson FE (1969) Radar design principles. McGraw Hill, New York, NY, 626 pp

Nathanson FE, Reilly JP (1968) Radar precipitation echo experiments on temporal, spatial, and frequency correlation, IEEE Trans AES-4(4):505–514

North EM, Peterson AM (1973) RASS, a remote sensing system for measuring low-level temperature profiles. Bull Am Meteoreol Soc 54:912–920

Probert-Jones JR (1960) The analysis of Doppler radar echoes from precipitations. In: Proceedings of 8th weather radar conference. American Meteorological Society, Boston, MA, pp 377–385

Richter JH (1969) High resolution tropospheric radar sounding. Radio Sci 4:1261–1268

Riddle AC, Angevine WM (1992) Ground clutter removal from profiler spectra, STEP, In: Edwards B (ed) Fifth workshop on technical and scientific aspects of MST radar, Aberystwyth, Wales, UK, 6–9 Aug. 1991, SCOSTEP, pp 418–420

Spizzich A (1974) Refraction of acoustic-waves in atmosphere and its influence on measurement of wind by SODAR Ann Telecommun 29:301–310

Spizzichino A (1974) Discussion of operating-conditions of a Doppler SODAR. J Geophys Res 79:5585–5591

Strauch RG, Merritt DA, Moran KP, Earnshaw KB, van de Kamp D (1984) The Colorado wind profiling network. J Atmos Ocean Technol 1:37–49

White AB (1997) Radar remote sensing of scalar and velocity microturbulence in the convective boundary layer. NOAA Tech. Memo. ERL ETL-276. Environmental Technology Laboratory, Boulder, CO. 127 pp. [Available from NOAA/ERL/ETL Broadway, Boulder, CO, 80305]

Wilczak JM, Gossard EE, Neff WD, Eberhard WL (1996): Ground-based remote sensing of the atmospheric boundary layer: 25 years of progress. Boundary-Layer Meteorol 78:321–349